Electronic Supplementary Material (ESI) for CrystEngComm.

A new series of trivalent lanthanide (Ce, Pr, Nd, Sm, Eu, Gd, Tb, Dy) coordination polymers with the 1,2-cyclohexanedicarboxylate linker: synthesis, crystal structure, luminescence and catalytic properties

Samantha E. Russell,[a] Cyrille Gosset,[a] Xavier Agache,[a] Christophe Volkringer,[ab] Natacha Henry,[a] Roel Decadt,[c] Rik Van Deun,[c] Marc Visseaux[a] and Thierry Loiseau*[a]

[a]*Unité de Catalyse et Chimie du Solide (UCCS) – UMR CNRS 8181, Université de Lille, ENSCL, Bat C7, BP 90108, 59652 Villeneuve d'Ascq, France,*
[b]*Institut Universitaire de France (IUF), 1,rue Descartes, 75231 Paris, France.*
[c]*Luminescent Lanthanide Lab (L^3), Department of Inorganic and Physical Chemistry, Ghent University, Krijgslaan 281, S3, 9000 Ghent, Belgium.*

* To whom correspondence should be addressed. E-mail: thierry.loiseau@ensc-lille.fr. Phone: (33) 3 20 434 434, Fax: (33) 3 20 43 48 95

SUPPLEMENTARY INFORMATION

To be submitted to CrystEngComm.
Version january 2016
Revised version February 24, 2016

FIGURES

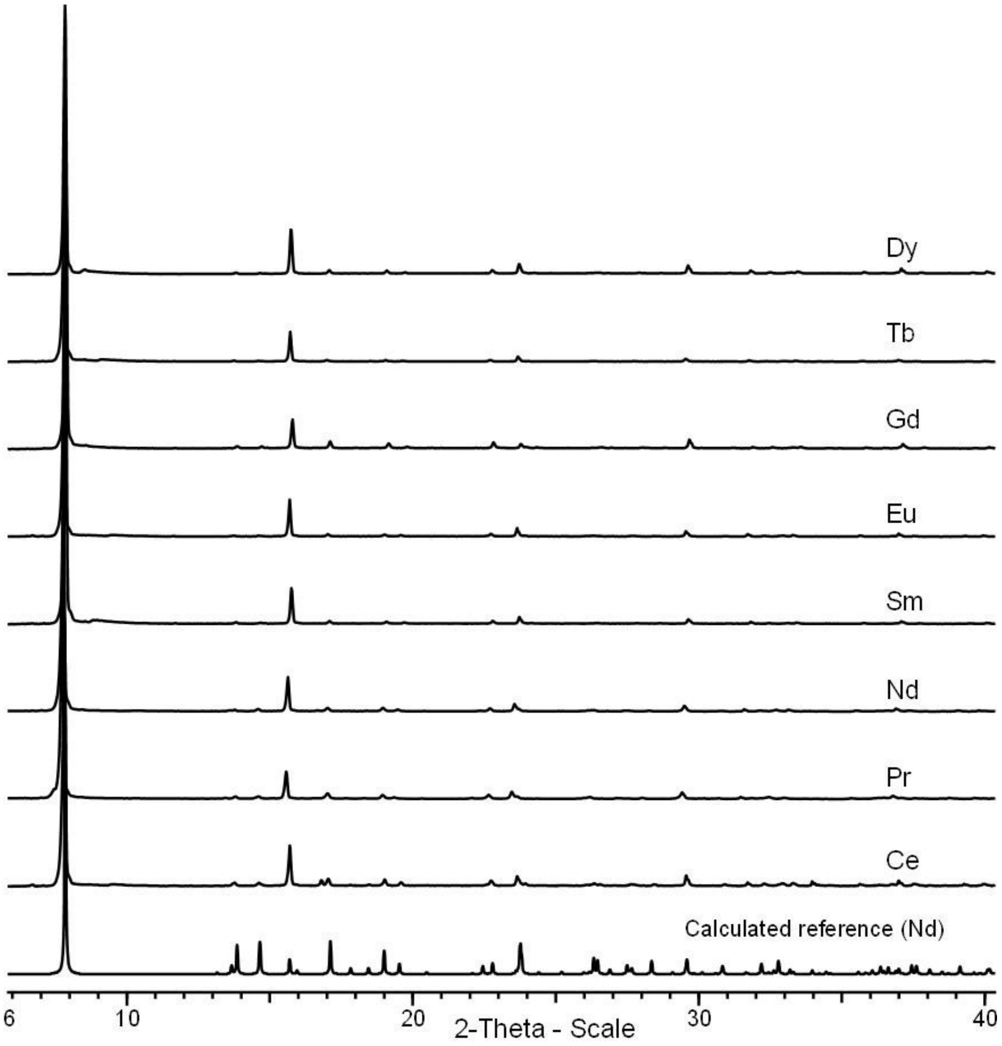

Figure S1a: Comparison of calculated and experimental X-ray powder patterns of Ln(1,2-chdc)(form)(H_2O); Ln = Ce^{3+} (**1**), Pr^{3+} (**2**), Nd^{3+} (**3**), Sm^{3+} (**4**), Eu^{3+} (**5**), Gd^{3+} (**6**), Tb^{3+} (**7**) and Dy^{3+} (**8**), 2θ scale, copper radiation. Calculated reference is from the Nd-based single-crystal XRD analysis. Change of Bragg peak intensity is due to preferential orientation of crystallites. For Ce-containing compound, an additional week Bragg peak is observed at 16.5° (2θ), which does belong to the powder XRD pattern of the phase **1**, and could be assigned to an unknown impurity.

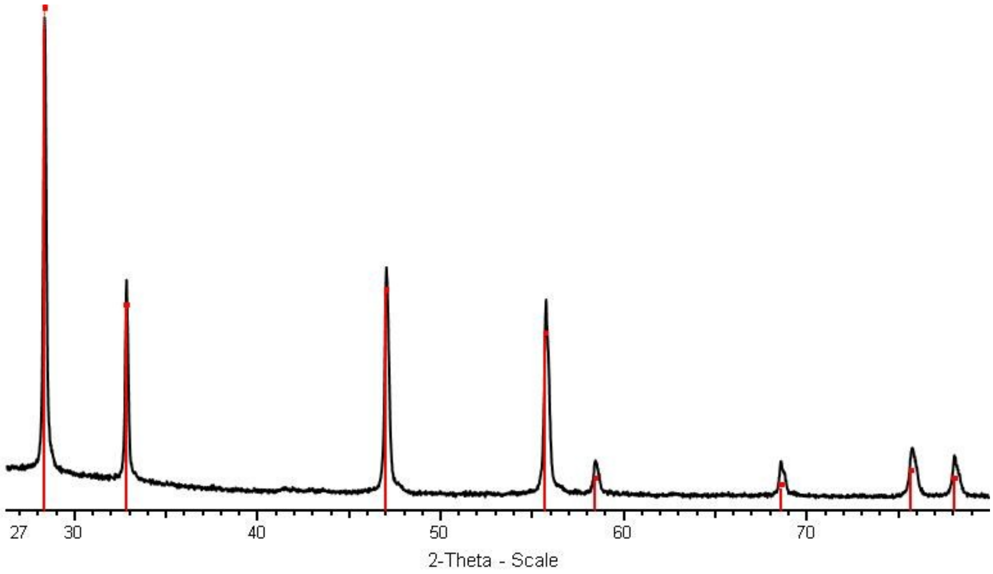

Figure S1b: experimental (black) and calculated (red, pdf number: 42-1121) X-ray powder patterns of Pr_6O_{11}. Pr_6O_{11} compound corresponds to the residue generated by the thermogravimetric analysis of compound **2**.

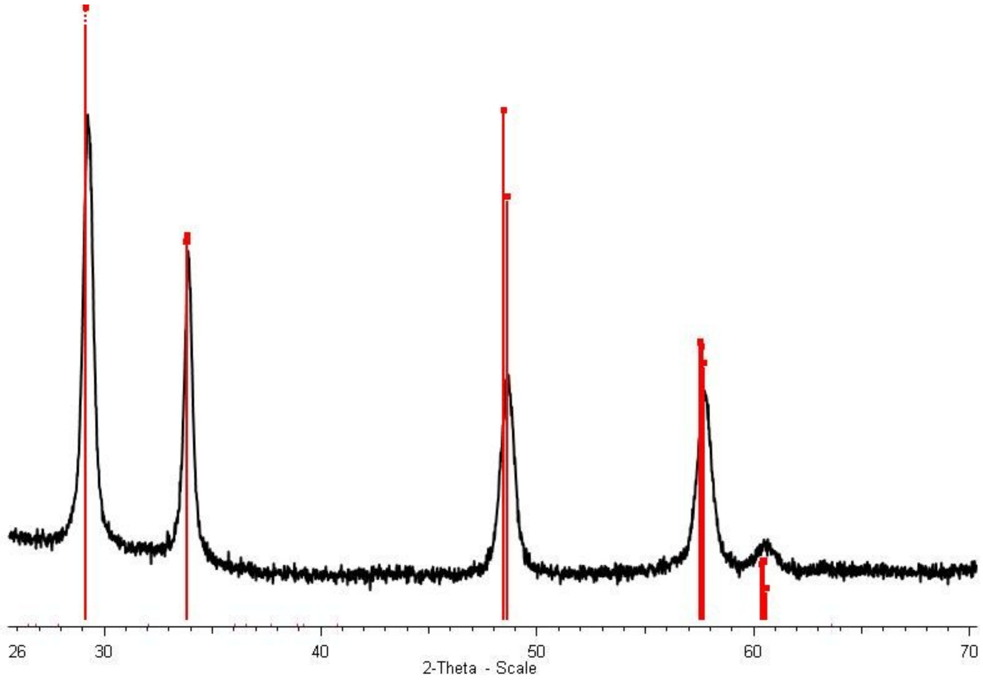

Figure S1c: experimental (black) and calculated (red, pdf number: 65-4511) X-ray powder patterns of $Tb_{11}O_{20}$. $Tb_{11}O_{20}$ corresponds to the residue generated by the thermogravimetric analysis of compound **7**.

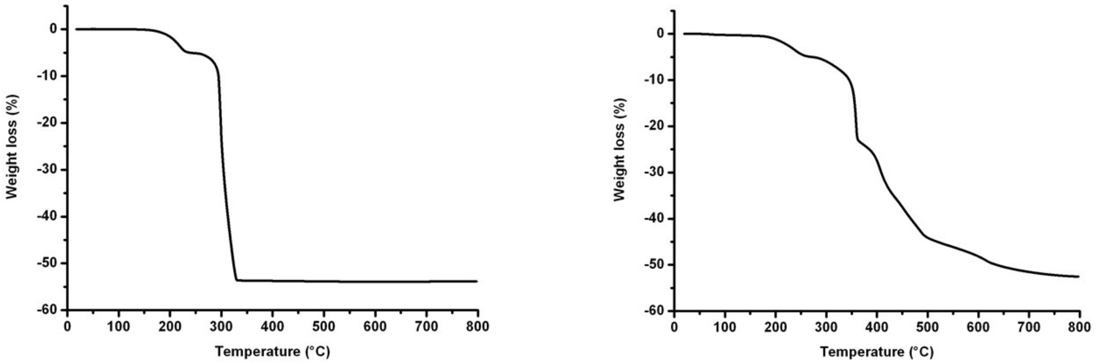

Figure S2a: Thermogravimetric curve of phases **1 (Ce**; left**)** and **2 (Pr**; right**)** under air atmosphere (heating rate: 1°C/min).

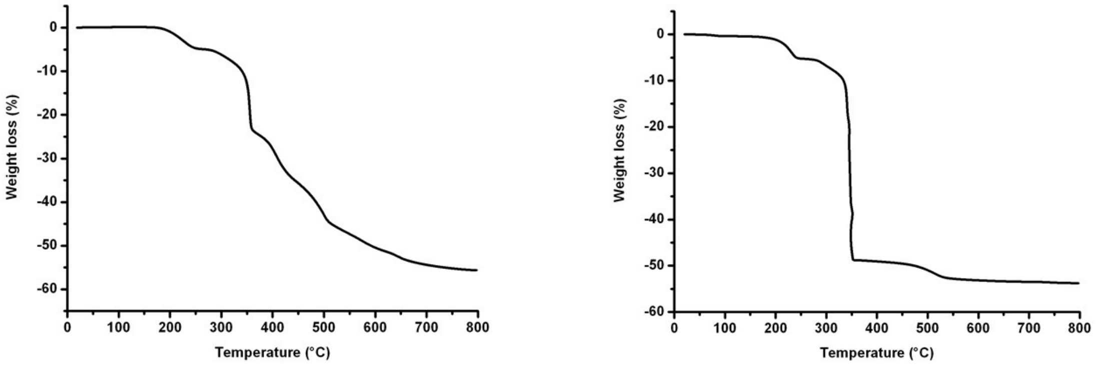

Figure S2b: Thermogravimetric curve of phases **3 (Nd**; left**)** and **4 (Sm**; right**)** under air atmosphere (heating rate: 1°C/min).

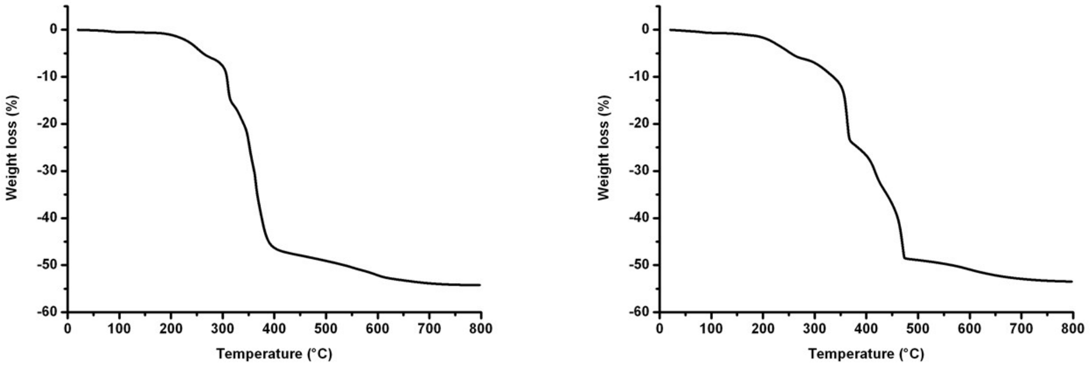

Figure S2c: Thermogravimetric curve of phases **5 (Eu**; left**)** and **6 (Gd**; right**)** under air atmosphere (heating rate: 1°C/min).

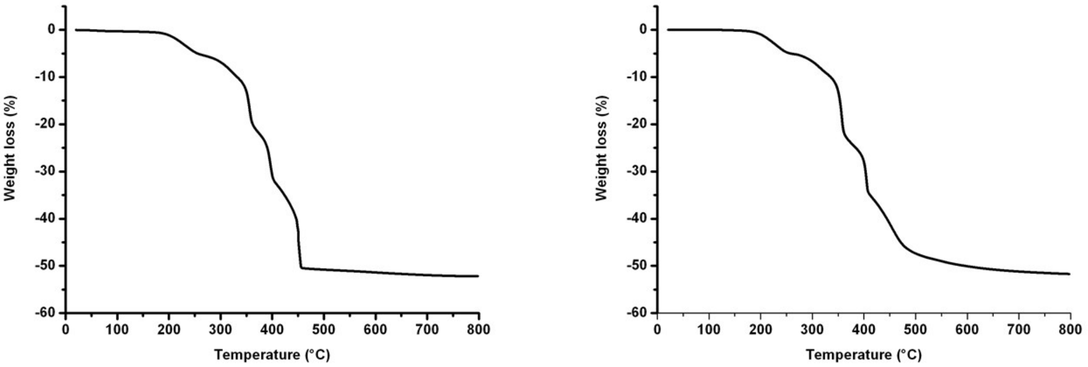

Figure S2d: Thermogravimetric curve of phases **7 (Tb**; left**)** and **8 (Dy**; right**)** under air atmosphere (heating rate: 1°C/min).

TABLES

Table S1: **Experimental and calculated weight loss values from thermogravimetric curves of compounds 1-8.**

Compound	First step[a] Calc.	First step[a] Obs.	Remaining weight[b] value Calc.	Remaining weight[b] value Obs.
1 (Ce)	4.8 %	5.0 % 240°C	44.0 % (Ce_2O_3) 46.1% (CeO_2)	46.2 %
2 (Pr)	4.8 %	4.8 % 260°C	45.5 % (Pr_6O_{11})	47.5%
3 (Nd)	4.8 %	4.7% 250°C	44.6 %	44.4%
4 (Sm)	4.7 %	4.9% 240°C	45.4 %	46.3 %
5 (Eu)	4.7 %	4.9 % 260°C	45.7 %	45.8 %
6 (Gd)	4.6 %	5.3% 260°C	46.4 %	46.5 %
7 (Tb)	4.6 %	5.2 % 260°C	46.7 % (Tb_2O_3) 48.2 % ($Tb_{11}O_{20}$)	47.8 %
8 (Dy)	4.6 %	4.7 % 250°C	47.1 %	48.3 %

[a] weight loss corresponding to the departure of 1 H_2O.

[b] calculations based on the Ln_2O_3 residue (Ln = Ce-Dy). For Ce, Pr and Tb, other dense oxides are also known to be formed at high temperature; corresponding stoiechiometries Ln_xO_y also mentioned, related to the remaining weight loss values.

X-ray thermodiffraction. X-ray thermodiffractometry of the compound **3** (Nd) was performed under 5L h^{-1} air flow in an Anton Paar HTK1200N of a D8 Advance Bruker diffractometer (θ-θ mode, CuKα radiation) equipped with a Vantec1 linear position sensitive detector (PSD). Each powder pattern was recorded in the range 6-35° (2θ) (at intervals of 20°C up to 600°C) with a 0.34s/step scan, corresponding to an approximate duration of 35mn. The temperature ramps between two patterns were 0.05°C.s^{-1} up to 600°C.

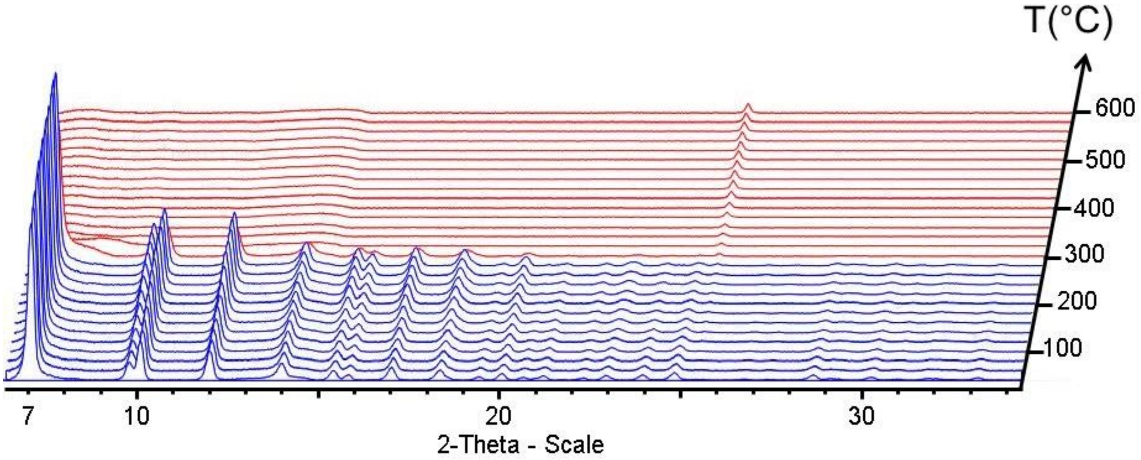

Figure S3: Powder X-ray thermodiffractogram of Nd(1,2-chdc)(form)(H_2O) (**3**), collected in the range of temperature (40-600°C) under air atmosphere.

Infrared spectroscopy. Infrared spectra of compound **1-8** were measured on Perkin Elmer Spectrum Two^{TM} spectrometer between 4000 and 400 cm^{-1}, equipped with a diamond Attenuated Total Reflectance (ATR) accessory.

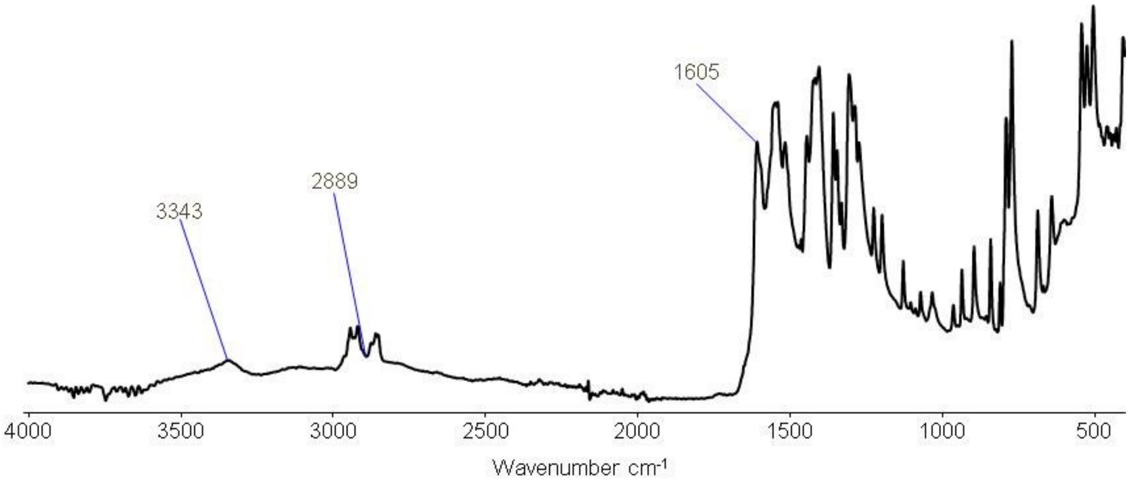

Figure S4a: Infrared spectrum of Ce(1,2-chdc)(form)(H_2O) (**1**).

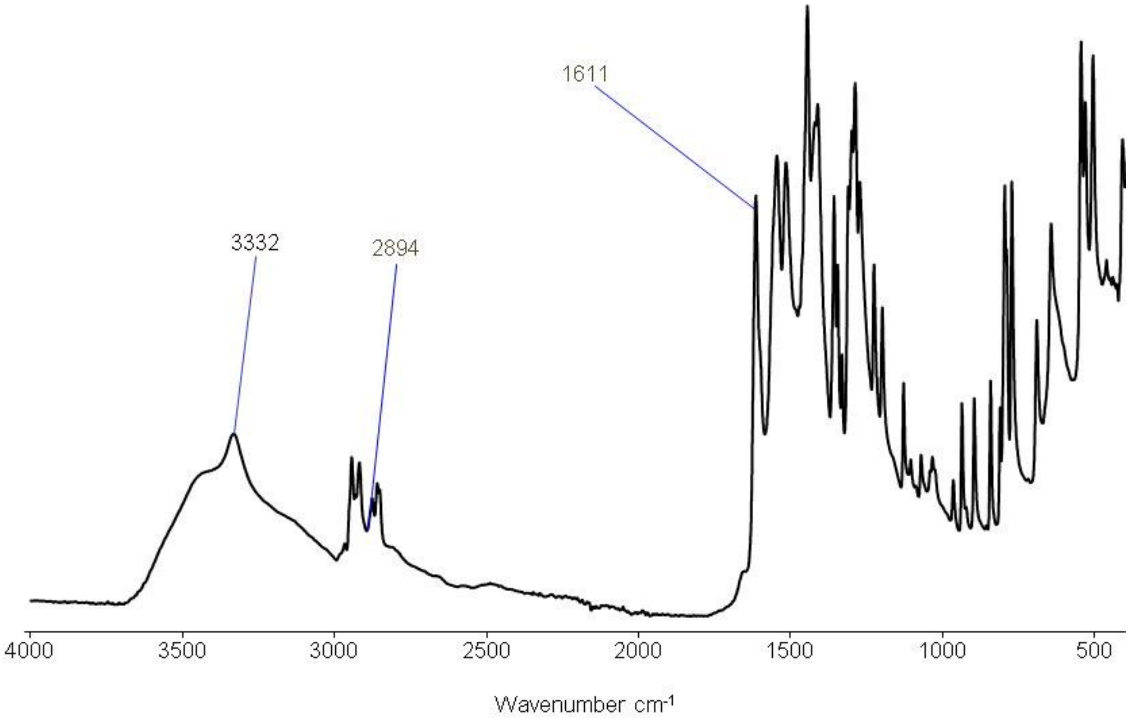

Figure S4b: Infrared spectrum of Pr(1,2-chdc)(form)(H_2O) (**2**).

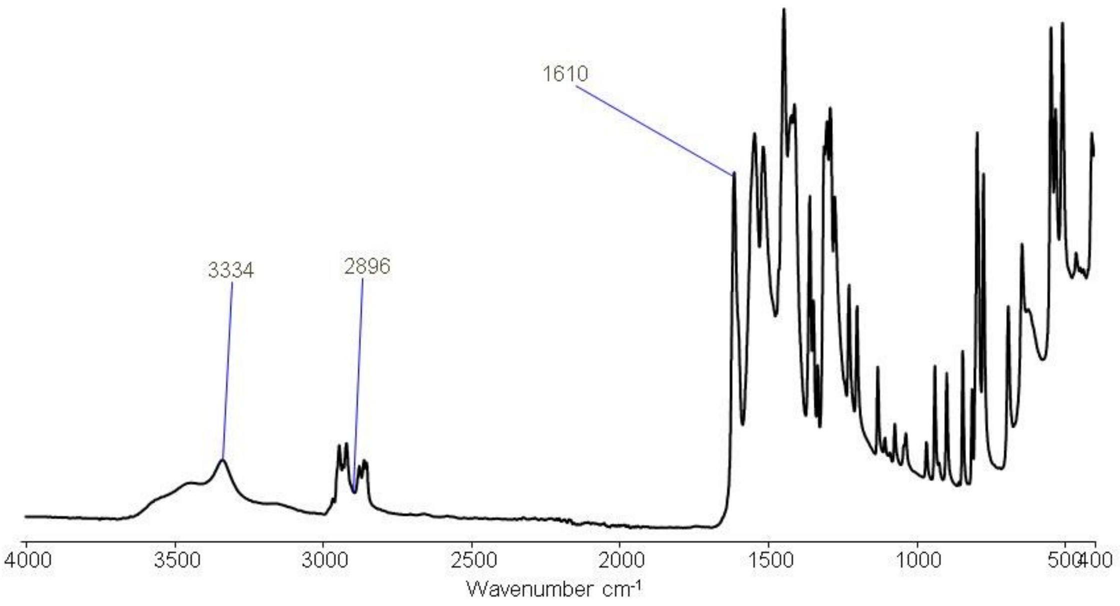

Figure S4c: Infrared spectrum of Nd(1,2-chdc)(form)(H_2O) (**3**).

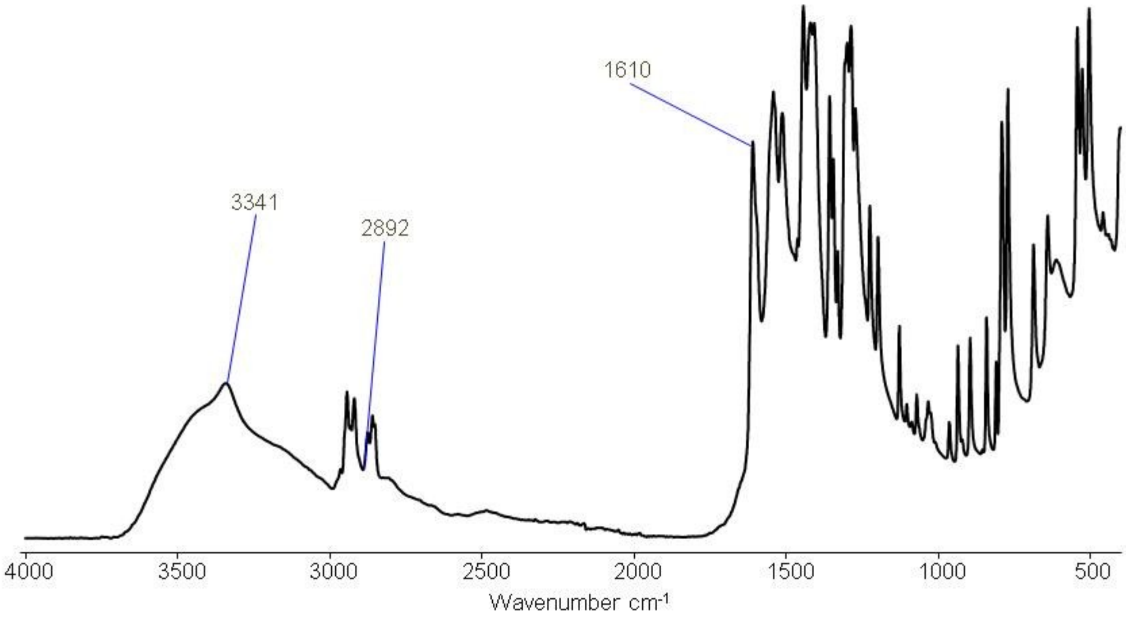

Figure S4d: Infrared spectrum of Sm(1,2-chdc)(form)(H_2O) (**4**).

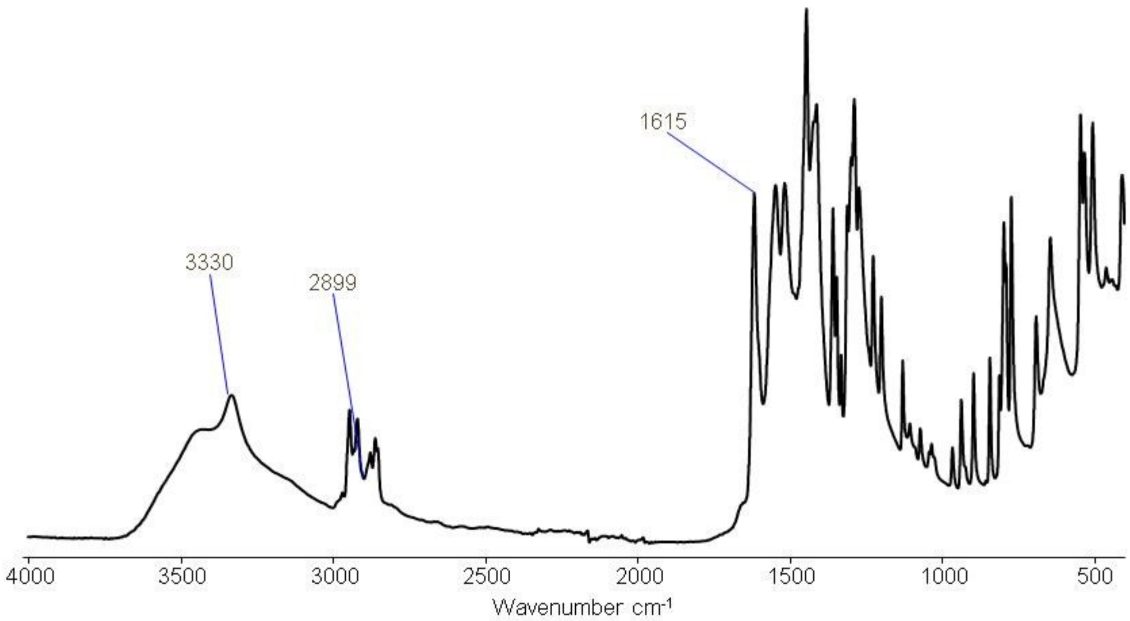

Figure S4e: Infrared spectrum of Eu(1,2-chdc)(form)(H_2O) (**5**).

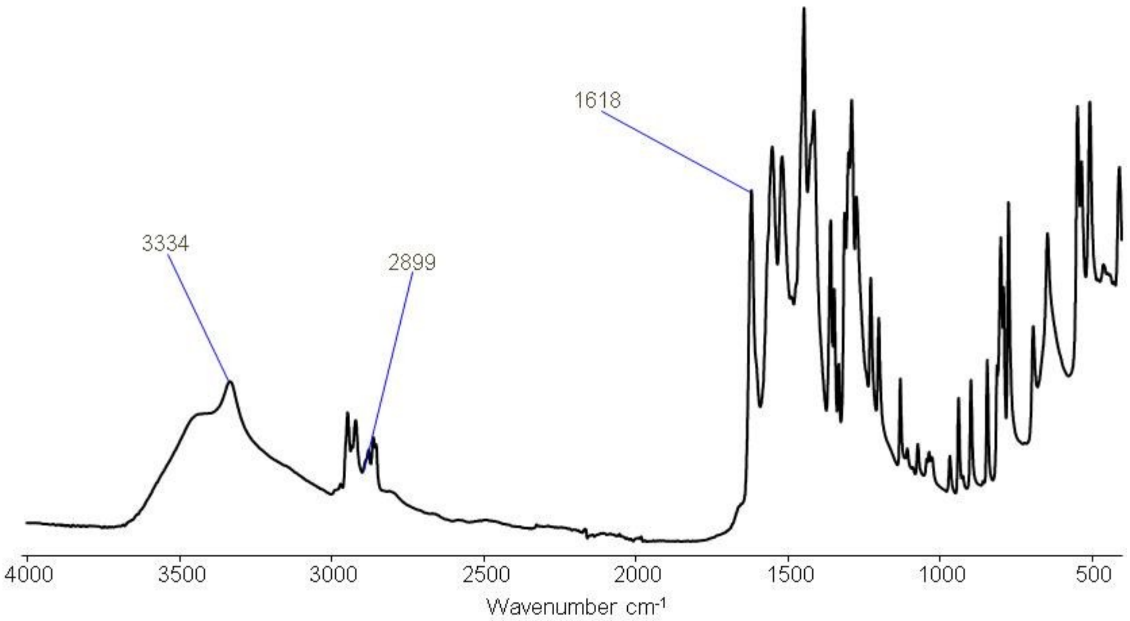

Figure S4f: Infrared spectrum of Gd(1,2-chdc)(form)(H_2O) (**6**).

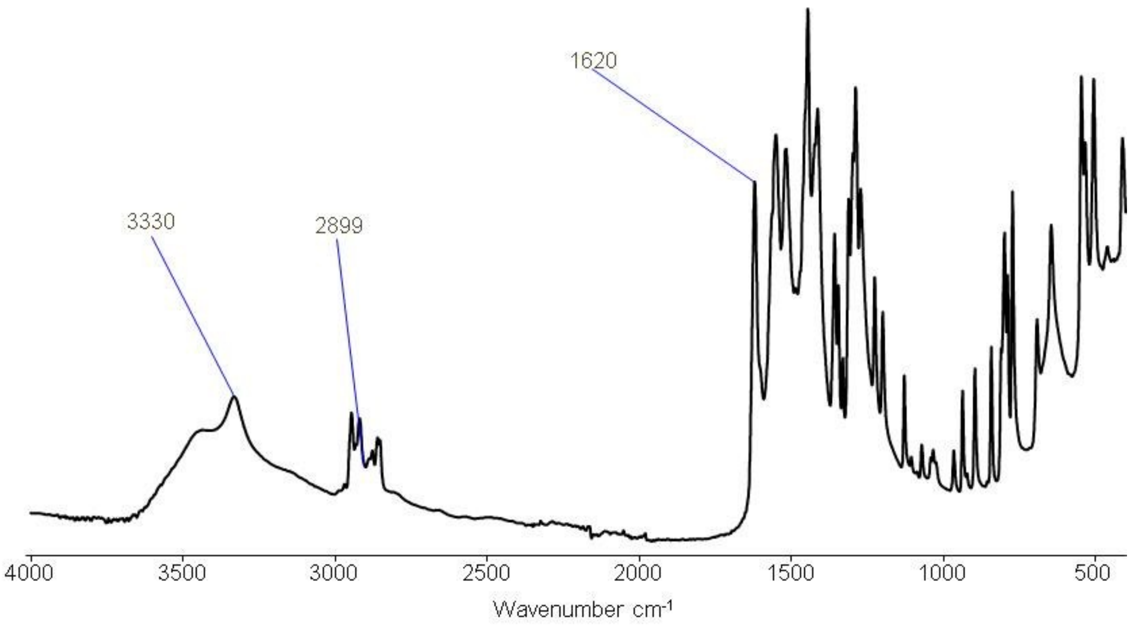

Figure S4g: Infrared spectrum of Tb(1,2-chdc)(form)(H_2O) (**7**).

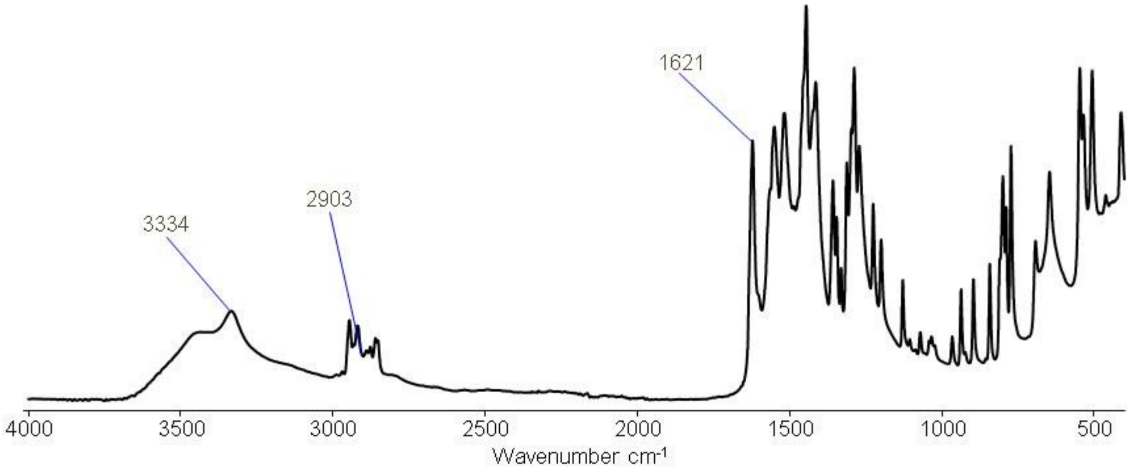

Figure S4h: Infrared spectrum of Dy(1,2-chdc)(form)(H_2O) (**8**).

On these spectra, we clearly identified at around:

- 3330 cm^{-1}, the vibration associated to the water molecule linked to the lanthanide
- 2920 and 2850 cm^{-1}, the vibrations corresponding to C-H vibrations of formate and cyclohexane dicarboxylate ligands, respectively.
- 1610 cm^{-1}, the band associated to the vibration of the carboxylate function C-O linked to the lanthanide center.

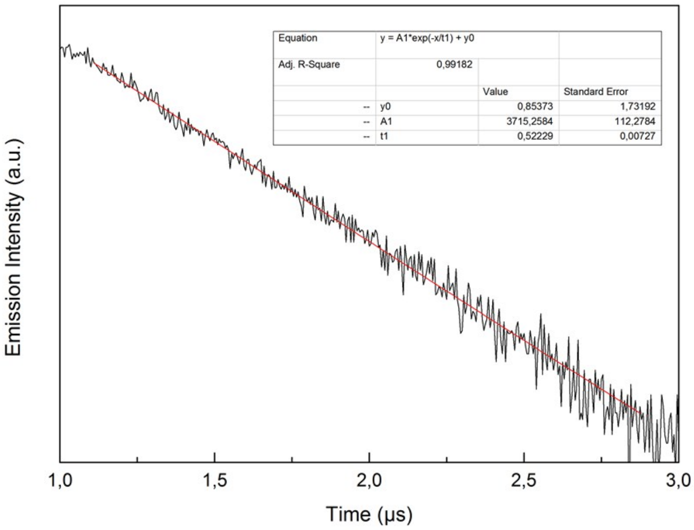

Figure S5: Mono-exponential decay curve from compound **1** (Ce), recorded at 445 nm upon excitation at 375 nm.

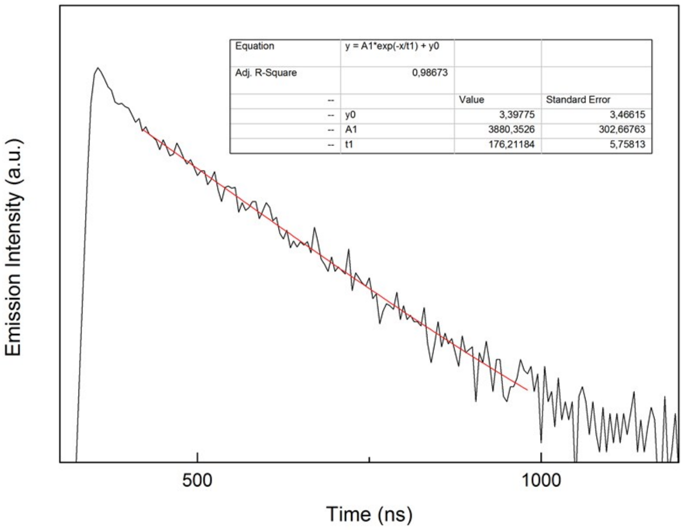

Figure S6: Mono-exponential decay curve from compound **3** (Nd), recorded at 1055 nm upon excitation at 353 nm.

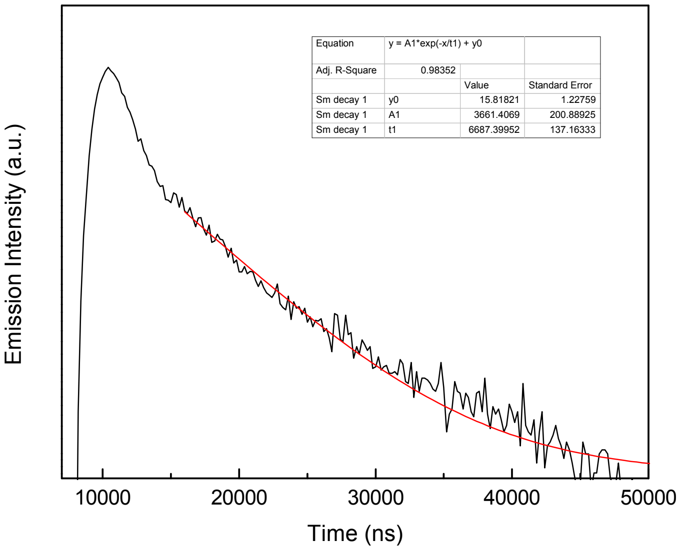

Equation	y = A1*exp(-x/t1) + y0		
Adj. R-Square	0.98352		
		Value	Standard Error
Sm decay 1	y0	15.81821	1.22759
Sm decay 1	A1	3661.4069	200.88925
Sm decay 1	t1	6687.39952	137.16333

Figure S7: Mono-exponential decay curve from compound **4** (Sm), recorded at 598 nm upon excitation at 401 nm.

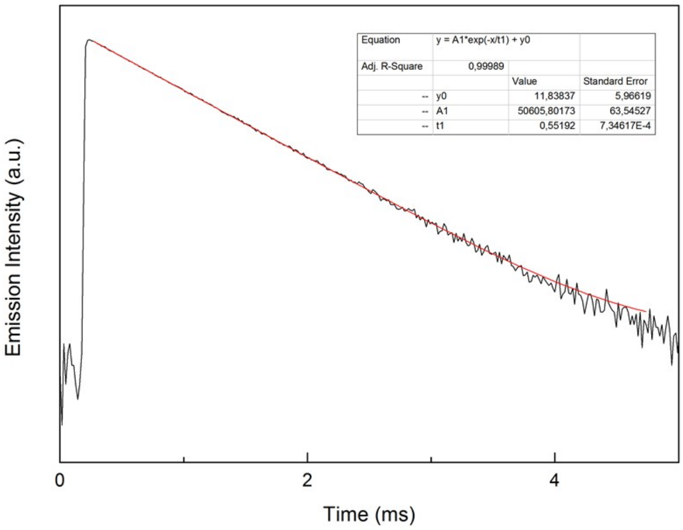

Equation	y = A1*exp(-x/t1) + y0		
Adj. R-Square	0,99989		
		Value	Standard Error
--	y0	11,83837	5,96619
--	A1	50605,80173	63,54527
--	t1	0,55192	7,34617E-4

Figure S8: Mono-exponential decay curve from compound **5** (Eu), recorded at 618.5 nm upon excitation at 393 nm.

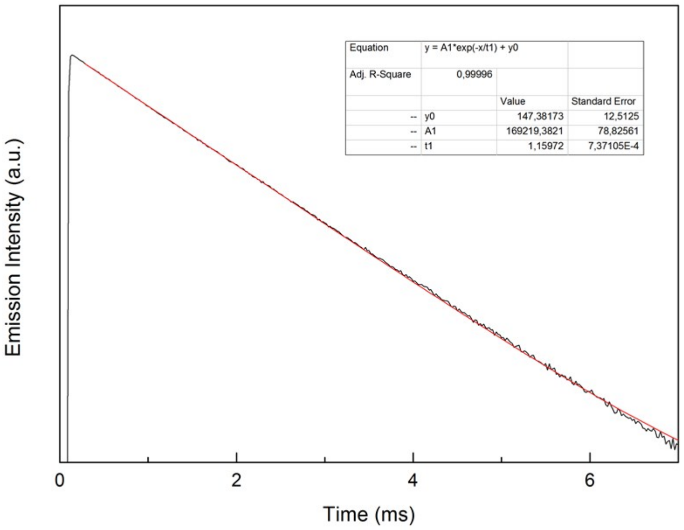

Equation	y = A1*exp(-x/t1) + y0		
Adj. R-Square	0,99996		
		Value	Standard Error
--	y0	147,38173	12,5125
--	A1	169219,3821	78,82561
--	t1	1,15972	7,37105E-4

Figure S9: Mono-exponential decay curve from compound **7** (Tb), recorded at 545 nm upon excitation at 351.5 nm.

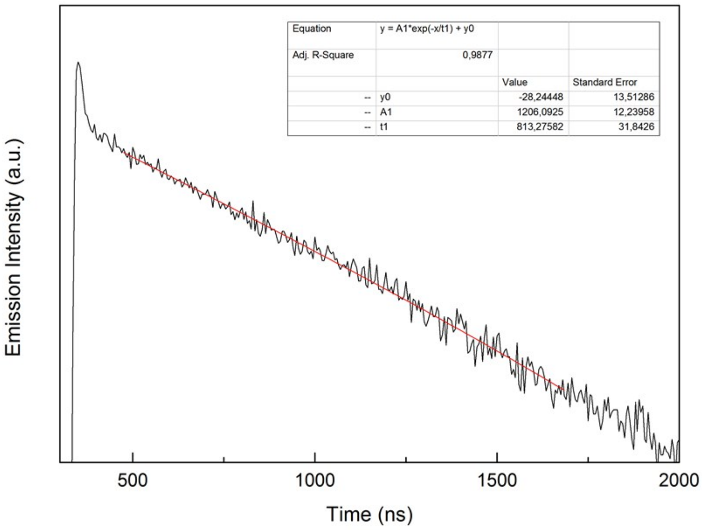

Equation	y = A1*exp(-x/t1) + y0		
Adj. R-Square	0,9877		
		Value	Standard Error
--	y0	-28,24448	13,51286
--	A1	1206,0925	12,23958
--	t1	813,27582	31,8426

Figure S10: Mono-exponential decay curve from compound **8** (Dy), recorded at 573.5 nm upon excitation at 351 nm.

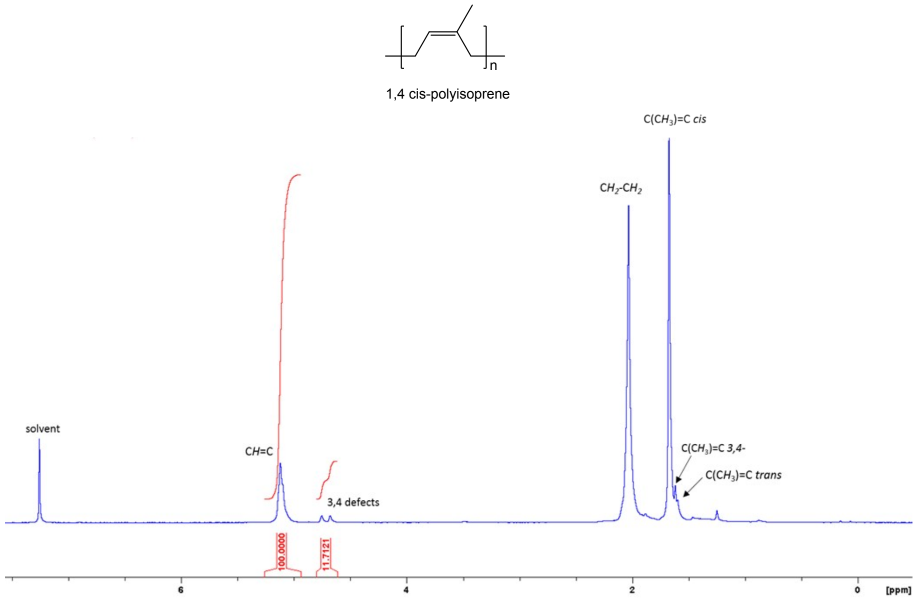

Figure S11: ^{1}H NMR spectrum of polyisoprene 93 % *cis*-regular obtained with compound **3** as pre-catalyst (solvent $CDCl_3$).